Arch. Metall. Mater. **67** (2022), 4, 1349-1354

DOI: https://doi.org/10.24425/amm.2022.141061

NURUL AIDA MOHD MORTAR[1,2], MOHD MUSTAFA AL BAKRI ABDULLAH[1,2*], KAMARUDIN HUSSIN[1], RAFIZA ABDUL RAZAK[3], SANUSI HAMAT[4], AHMAD HUMAIZI HILMI[4], NOORFIFI NATASHA SHAHEDAN[1], LONG YUAN LI[5], IKMAL HAKEM A AZIZ[1]

FINITE ELEMENT ANALYSIS ON STRUCTURAL BEHAVIOUR OF GEOPOLYMER REINFORCED CONCRETE BEAM USING JOHNSON-COOK DAMAGE IN ABAQUS

This paper details a finite element analysis of the behaviour of Si-Al geopolymer concrete beam reinforced steel bar under an impulsive load and hyper velocity speed up to 1 km/s created by an air blast explosion. The initial torsion stiffness and ultimate torsion strength of the beam increased with increasing compressive strength and decreasing stirrup ratio. The study involves building a finite element model to detail the stress distribution and compute the level of damage, displacement, and cracks development on the geopolymer concrete reinforcement beam. This was done in ABAQUS, where a computational model of the finite element was used to determine the elasticity, plasticity, concrete tension damages, concrete damage plasticity, and the viability of the Johnson-Cook Damage method on the Si-Al geopolymer concrete. The results from the numerical simulation show that an increase in the load magnitude at the midspan of the beam leads to a percentage increase in the ultimate damage of the reinforced geopolymer beams failing in shear plastic deformation. The correlation between the numerical and experimental blasting results confirmed that the damage pattern accurately predicts the response of the steel reinforcement Si-Al geopolymer concrete beams, concluded that decreasing the scaled distance from 0.298 kg/m^3 to 0.149 kg/m^3 increased the deformation percentage.

Keywords: Fly ash geopolymer; geopolymer concrete; finite element analysis; Johnson cook damage; ABAQUS software

1. Introduction

Geopolymers was introduced by Davidovits (1978) as a replacement binder to ordinary Portland cement (OPC). The use of conventional cement involves a higher amount of emission of greenhouse gases (CO_2) when manufacturing OPC, and geopolymer technology has the potential of reducing CO_2 emissions [1-2]. Geopolymers can be made from materials with high percentages of alumina (Al_2O_3) and silica (SiO_2), such as fly ash, kaolin, rice husk ash, slag, metakaolin, and bottom ash. The raw materials are mixed with an alkali activator such as sodium hydroxide to obtain a geopolymer gel [3-6]. The gel is known as a non-cementitious binder, as it binds the coarse and fine aggregates and other additive materials in the mixture to form a geopolymer concrete [7]. Geopolymers have excellent mechanical properties, high early strength, high energy absorption capacity, low shrinkage and creep, and excellent thermal resistance [8-10].

The advantages of geopolymers relative to its conventional counterpart are that it enhances the strength of protective structures and durability of buildings under extreme loads when incorporated into these structures. Attempts to use geopolymers as a high-performance concrete have been analysed via steel bar reinforced with Si-Al geopolymer concrete beams. There is a lack of research on the behaviour of geopolymer concrete vis-à-vis high impact explosion pressure and studies on the impact of explosions on beams mainly focussed on the arrangement reinforcement or the addition of fibre reinforcement only occurring in the OPC concrete. Concrete blast testing was investigated to determine the strength and durability of concrete as protection barriers and bomb proofing materials [11]. Previous studies also reported experiments involving high explosion tests, where the standoff distances were gradually decreased in their quest to quantify the concretes' capacity for absorbing energy and its corresponding shear strength [12]. The explosion phenomenon of the OPC was discovered via a range of tests encompassing

[1] UNIVERSITI MALAYSIA PERLIS, CENTER OF EXCELLENCE GEOPOLYMER AND GREEN TECHNOLOGY (CEGEOGTECH), MALAYSIA
[2] UNIVERSITI MALAYSIA PERLIS (UNIMAP), FACULTY OF CHEMICAL ENGINEERING TECHNOLOGY, MALAYSIA
[3] UNIVERSITI MALAYSIA PERLIS (UNIMAP), FACULTY OF CIVIL ENGINEERING TECHNOLOGY, MALAYSIA.
[4] UNIVERSITI MALAYSIA PERLIS (UNIMAP), FACULTY OF MECHANICAL ENGINEERING TECHNOLOGY, MALAYSIA
[5] UNIVERSITY OF PLYMOUTH, SCHOOL OF MARINE SCIENCE AND ENGINEERING, PLYMOUTH PL4 8AA, UNITED KINGDOM
* Corresponding author: mustafa_albakri@unimap.edu.my

dynamic bending, and shear and indirect stress post-explosive detonations executed at different damage levels [13].

Blast field experiments involving explosives are not repeatable due to prevalent experimental risks in dealing with explosives. Numerical modelling, on the other hand, allows researchers to investigate multiple design parameters at a significantly lower cost (and risks). Finite element models can be used to describe the shear failure mechanism of reinforced concrete beams to a level that is similar to a real test [15]. The results that can be obtained from software simulation include the expected stirrup yielding, beam cracking, and the stress distribution of compressive and tensile stresses of the reinforced steel bars concrete beam [16]. The finite volume, finite difference, finite element property, and mesh methods can be used to elucidate the damage mechanisms and for the development of other finite analyses models [17,18].

There is a lack of studies involving the performance of geopolymer reinforcement concrete structures under explosion loading using ABAQUS. Thus, the development of a finite element model (FEM) using Johnson Cook Damage for simulating damages after high impact loading using the damaged plasticity model is useful for many materials. It is essential to arrest crack initiation to prevent concrete structures from being further damaged, especially in the case of construction structures. This paper analyses the geopolymer concrete beams by mainly focussing on the different loadings caused by explosions by comparing the damages in the Johnson-Cook Damage model in the ABAQUS software.

2. Blasting exposure experiment

A blast event was executed to examine the response of the concrete panels towards the air blast explosion, and its configuration is shown in Fig. 1. The GCRB beam measures 100 mm in height, 100 mm in width, and 1100 mm in length, and has simple support at each end. The compression concrete tests reported a strength of 80 MPa for the geopolymer concrete. An explosive expert from the Malaysian Military Explosive Unit executed the test at an undisclosed military facility, as per the TM5-1300 (1990). A cylindrical Emulex explosive charge (0.30 kg) was hung over the midspan test specimens with vertical standoff distance, as shown in TABLE 1.

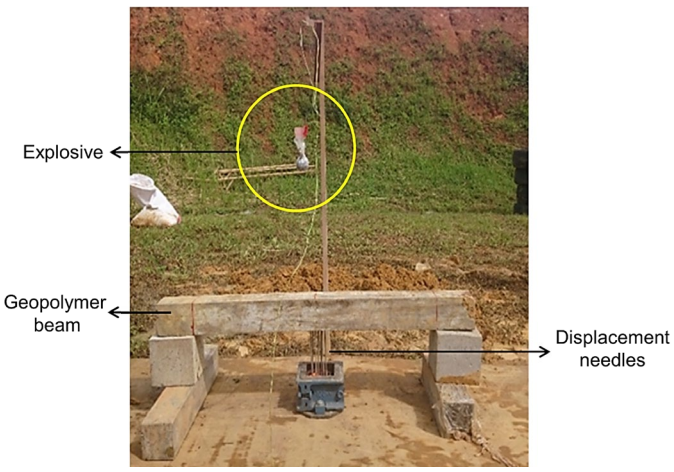

Fig. 1. Blast field experiment set up

TABLE 1

Parameter for air blasting

Specimen	Mass of Explosive (kg)	Standoff Distance (mm)	Scaled Distance (kg/m^3)
GCRB 1	0.3	200	0.298
GCRB 2	0.3	150	0.224
GCRB 3	0.3	100	0.149

3. Finite element model

3.1. Material property model

The geopolymer beam model was developed using ABAQUS to simulate damage levels at various loadings on a (similar) beam. Three reinforcing beam patterns; GCRB 1, GCRB 2, and GCRB 3, were investigated using explicit analysis. The beam is efficient for solving simulated crashes or impacts on nonlinear materials and large deformations. Both the geometric and material properties were inputted into the numerical simulations, and the stress-strain relationships for the steel bar, stirrup, and concrete beam was assumed to be perfectly plastic and elastic. The perfectly plastic-elastic data define the true yield stress of the material as a function of true plastic-elastic strain. The first piece of data given defines the initial yield stress of the material and, therefore, should have a plastic strain value of zero. Perfectly plastic-elastic material cause the stress and strain increases up till the yield points then the stress become constant while the strain increase. In the case of the concrete, concrete in the damaged plasticity model is suitable for representing the complete inelastic behaviour of concrete with tension and compression, which makes it viable for damage simulation [19-21]. The effective tensile and compressive cohesion stresses can be determined using the following Eq. 1 and Eq. 2 [22]. The correlation of tensile and compressive stress-strain curve is characterized by two damage variables that is d_t and d_c.This values can be from zero which is represents the undamaged materials where one represents total loss of strength. E_0 is the initial elastic stiffness of the material and $\acute{\varepsilon}_c^{pl}$, $\acute{\varepsilon}_t^{pl}$, ε_c, ε_t are compressive plastic strain, tensile plastic strain, compressive inelastic strain and tensile inelastic strain respectively.

$$\bar{\sigma}_t = \frac{\sigma_t}{1-d_t} = E_0\left(\varepsilon_t - \acute{\varepsilon}_t^{pl}\right) \tag{1}$$

$$\bar{\sigma}_c = \frac{\sigma_c}{1-d_c} = E_0\left(\varepsilon_c - \acute{\varepsilon}_c^{pl}\right) \tag{2}$$

TABLE 2 shows the material parameter for the reinforced steel bar used in the geopolymer steel bar reinforced concrete.

TABLE 2

Parameter for reinforcement steel bar

Parameter	Poison ratio	0.34
	Tensile Strength	420 N/mm^2
	Yield strength	350 N/mm^2
	Thermal conductivity	51.9 W/(m.k)
	Melting temperature	1058°C
	Elastic modulus	20500 N/mm^2
	Shear Modulus	81800 N/mm^2
	Density	7830 kg/m^3
	Strain rate	0.014

3.2. The meshing of concrete and reinforcement

A 10×10 mesh size of eight-node linear brick elements was generated in ABAQUS in the beam analysis. The linear hexagonal element dilation on the mesh has been implemented due to the excellent agreement between the results of the study, and the experimental data indicated that the mesh is acceptable for generating accurate total response parameters. The same meshes were used without considering the sensitivity of the results to mesh refinement. The type of C3 D8R elements was performed via integration reduction. Six integration points were used throughout the 100 mm thickness of the beam matrix to establish the development of plasticity damage and to ensure that failure is modelled sufficiently. The reduced integration will result in a different stiffness matrix that will be rank-deficient due to the number of rigid-body modes of the hourglass modes. The cross-section area is modelled using layers of the uniaxial reinforcement steel bar. The boundary conditions of symmetry were imposed on the four edges of the mesh and in the transverse direction.

3.3. Boundary condition and loading of geopolymer concrete beam

The process of developing the FEM in the geopolymer beam was divided into two distinct steps. First, the geopolymer concrete beam and reinforcing bars were created as separate parts in the graphical interface of the program. At the two ends of the beam, pins were set to signify its fixed positions. The blasting model, known as the Eulerian body, included the concrete, reinforcement, blast area, and explosive. The Blast area was declared as air, and combined with two different materials between ideal gas and explosives. The detonation point was set up at the middle of the beam and the center part of the explosive.

Two models were assembled for the heat transfer analysis as part of the sequential analysis process, and the second for stress analysis taking into account the thermal effects. The configuration of the model was identical for the heat transfer, specific heat, viscosity, density, and the structural analysis stages. The number of elements and mesh configuration for the concrete and reinforcement assemblies must remain constant; otherwise, the data on nodal temperatures cannot be transferred accurately from the heat transfer analysis into stress analysis. The second step involves the determination of the thermo-mechanical properties for both assemblies. At this point, the model of heat transfer began distinguishing itself from the model of stress analysis in terms of element forms, boundary conditions, and blast loading

4. Results and discussion

4.1. Stress distribution and cracks development

The experimental and numerical results show where the parametric study of GCRB 1, GCRB 2, and GCRB 3 represent the effect of loads at the distributed stress, damage at midspan and cracking and scabbing, as well as strain rate effect in tension, respectively. In this approach, the problem mainly influenced by the two main failure mechanisms in concrete is the compressive stress crushing and tensile strain cracking. Loading styles and conditions primarily affect the crack pattern for any reinforced concrete structure. Generally, higher scaled distance causes the beam to be perfectly elastic, allowing it to sustain internal cracking and high rate dependant continuum damage as shown in Fig. 2. The cracks formed because of the structural failure known as shear failure due to shear force.

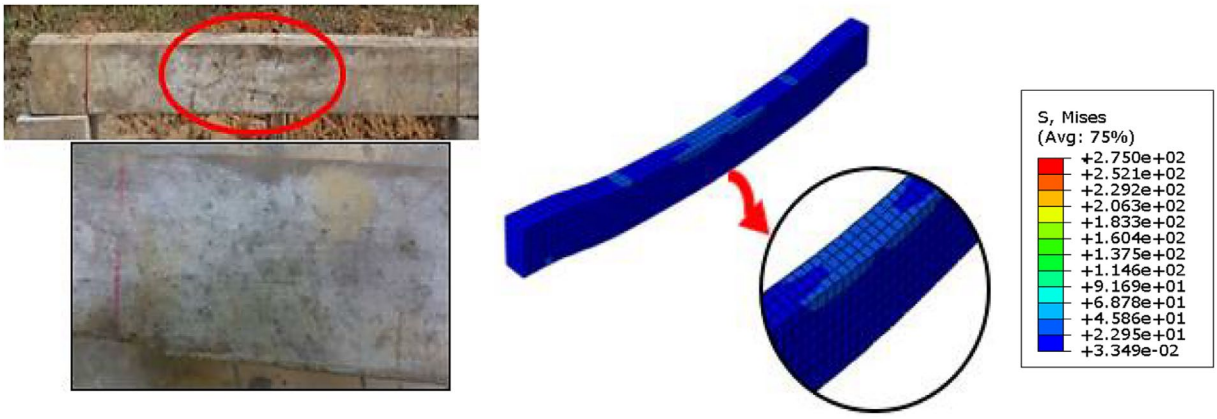

Fig. 2. Deformation of GCRB 1 after blasting on experimental and simulation

Shear failure develops more quickly at the edge middle of beam part because compressive strength at the top is lower and not strong to resist the distributed load. As the load increases, the micro cracks grow and meeting up into larger cracks and finally form the fracture zone. Coarse aggregate may prevent the crack growth which producing branching and meandering of the cracks. Early cracking initiation and propagation normally occur at the top mid height area and exfoliation occurs at the side cover concrete. The minor shear cracks are attributed to impact and reflective waves and the resulting peak of pressures, as well as the high strain rates experienced during blast test.

The distribution of many micro-cracks will lead to the first noticeable surface crack and concrete scabbing on GCRB 2 in Fig. 3. At each level of damage, the crack changes, and the strain rate deformation and concrete spallation of these beams had been visually investigated. It can be assumed that GCRB 3 is spalling out experimentally and the element is eroded in the numerical simulation because the two-point loads were flexural cracks and compressive damage on the bottom and top of the beam, respectively. The damage variable of the three beams is different, depending on the scaled distance for each parameter set up.

A detailed investigation is observed in concrete structures of GCRB 2, and obviously, failure occurred in the compressive and tension regions on GCRB 3 as shown in Fig. 4. The red colour on the beam stimulated that the higher concentration of energy is transferred after the detonation. By using the Johnson Cook model, the spallation of the concrete can be shown. In this case, the material's maximum capacity or strength is reached at the centre of the beam due to the shock focusing and high blast energy concentration. The number of pressure hits at the crack position point is higher than that of the two ends of the beam and is attributable to the increased stiffness of the beam. Apart from that, the beam's cross-sectional area's relatively high-pressure capacity can be attributed to the increasing damage level up to the ultimate failure. The majority of the cross-section ruptured at the midspan. The stimulated damage area and all forms of cracking are significant for understanding and regulating the different effects of exposure and long-term performance due to the impulsive loading and blast pressure.

Comparisons of the numerical and experimental results confirmed the excellent performance of the present model in predicting the effect of blast exposure. A computational analysis was performed to elucidate the dynamic behaviour of stress distribution from explosive detonation and structure failure phenomenon under the blast load on Si-Al geopolymer concrete. In the blasting phenomenon, the damage mode of beam is assumed from overall bending fracture to spallation damage and severe exfoliation with the increase of scaled distance. Through experimental study, the blast resistant performance and the

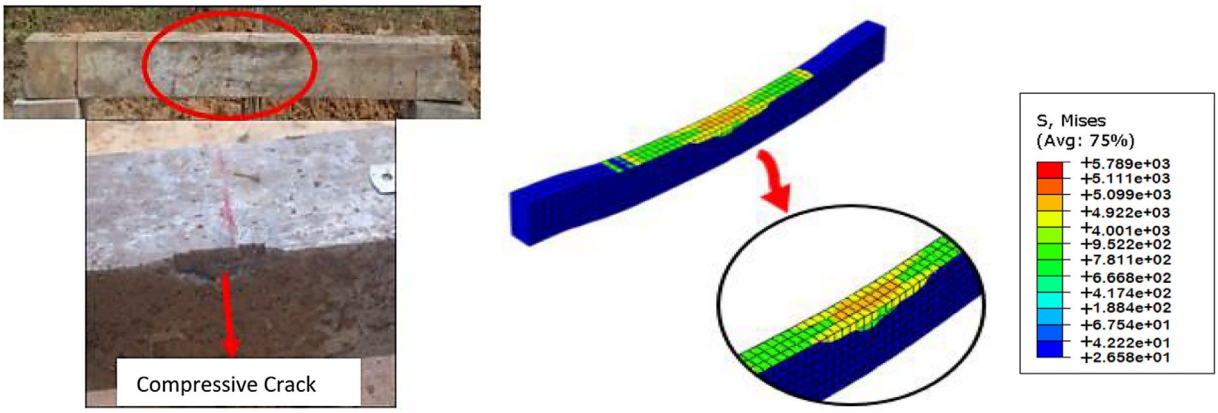

Fig. 3. Deformation of GCRB 2 after blasting on experimental and simulation

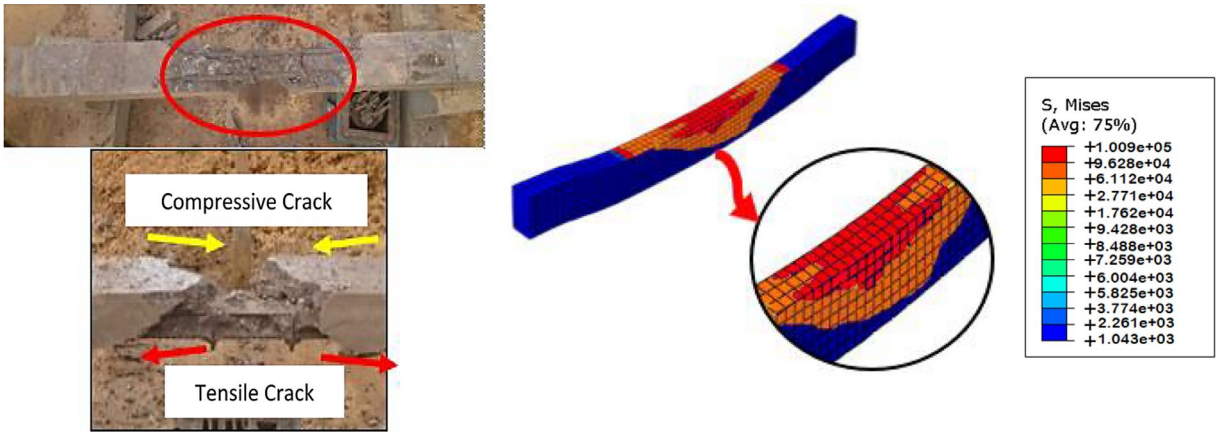

Fig. 4. Deformation of GCRB 3 after blasting on experimental and simulation

damage morphological feature and failure modes of reinforced concrete beam were analysed in details.

The FEM was first tested by simulating an earlier experimental blasting test. Following this, further parametric tests determining the effects of weights and positions of explosive charges, distances, concrete properties, types of initial cracks, cause of compressive and tensile failure, and longitudinal reinforcement ratios on the concrete beam's dynamic actions under air blast testing can be done via ABAQUS without needing to prepare samples to be tested at the blast sites.

4.2. Analysis of blast energy towards the beam

The response of the deformed model at the midspan is described using the total energy load of the system and drift response, as shown in Fig. 5. The simulation results and subsequent discussion focused on the energy used to control the hourglass deformation formed from the explosion that transformed the Si-Al geopolymer beams. The relationship of both the internal and kinetic energy reflects the vibrations towards beams tested under gravity, and without a confined space, the blasting load was in the air. The energy quantity in the beam model showed pinching, denoting the loss of strength and rigidity, and consequently low capacity for energy dissipation. Since the Si-Al geopolymer concrete was assigned as linear elastic, its total energy was conserved via the matrix. Energy output can provide valuable insight into model behaviour and artificial energy generated by internal hourglass forces. Large relative displacements on a contact interface within a time increment can lead to significant energy contributions.

Fig. 6 shows the energy load at the artificial strain energy on the specimen. Throughout the analysis, the response of the sample appears stiffer relative to the experimental response due to the possible changes as the refinement in the material model increases. By comparison, the hysteretic loops obtained, including the materials' rate dependency and damping from the analysis decreased the pinching effect when the Johnson-Cook plasticity damage analysis was performed in ABAQUS.

This can be identified by plotting the total energy of ALLDMD and ALLAE of the entire model. The assumption of perfect interactions between the concrete and reinforcement created problems in the hysteretic simulations in ABAQUS. The blast energy resulted the highest at 0.149 scaled distance in GCRB 3 that initiated at 0.35×10^6 N at 1 sec. Through the damage levels and damage modes of reinforced concrete beam under air blast explosion, the percentage difference was obtained by the experiment and simulation in range 7% to 20%.

5. Conclusions

This paper analysed the effects of dynamic loading on geopolymer concrete from the explosive blasting phenomenon by

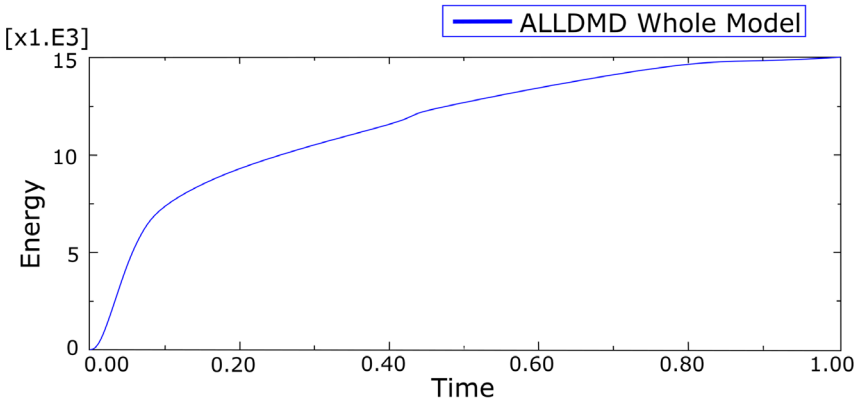

Fig. 5. Blast energy at the midspan

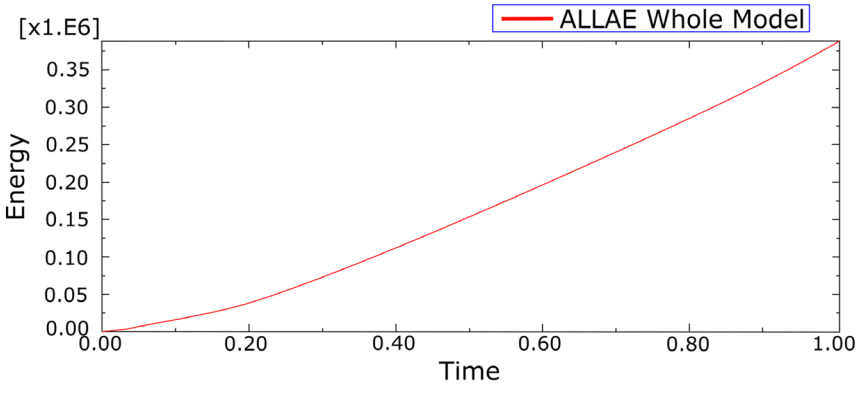

Fig. 6. Artificial strain energy on the beam

varying the scaled distance during the experiments and numerical studies. The structural behaviour of new concrete material from waste products was investigated by analysing the cracks' development, displacement, and stress distribution at each level of damage.

The compressive and tensile mode damages and failures due to the explosion of Si-Al geopolymer concrete were validated experimentally and numerically. It was found that decreasing the scaled distance from 0.298 kg/m^3 to 0.149 kg/m^3 of the capacity of the reinforced beam at the time of strengthening affected the stress distribution capacity. Although the geopolymer concrete is a viable replacement for the OPC, there is limited research that investigates its resistance towards blast loading. Thus, the following conclusions were made based on the analyses of the structural behaviour of the geopolymer concrete:

1. Visual observation showed that the failure occurred in the majority of compressive and tensile cracks for the beams at lower-scaled distances, particularly at the top and bottom of the middle beam, which was near the explosive energy source.
2. Analysing the structural behaviour at each scaled distance can help determine the damage levels and crack mode types, alongside the presence (if any) of a relationship between flexural and shear damages.
3. The Johnson-Cook plasticity model is useful in simulating the damage blast effect on geopolymer materials.

Acknowledgement

The authors wish to acknowledge the Center of Geopolymer and Green Technology for providing the laboratory facilities. This work was funding supported by the "Partnership for Research in Geopolymer Concrete" (PRIGeoC-689857) sponsored by the European Union.

REFERENCES

[1] J. Davidovits, Properties of geopolymer cements, First Int. Conf. Alkaline Cem. Concr. 131-149 (1994).

[2] K. Ramujee, M. Potharaju, Mechanical properties of geopolymer concrete composites, Mater. Today Proc. **4**, 2937-2945 (2017).

[3] I.H Aziz, M.M.A.B. Abdullah, C.Y. Heah, Y.M. Liew, Behaviour changes of ground granulated blast furnace slag geopolymers at high temperature, Adv. Cem. Res. **32**, 465-475 (2020).

[4] A.M.M. Al Bakri, H. Kamarudin, M. Bnhussain, I.K. Nizar, A.R. Rafiza, A.M. Izzat, Chemical Reactions in the Geopolymerisation Process Using Fly Ash-Based Geopolymer: A Review, J. Appl. Sci. Res. **7**, 1199-1203 (2011).

[5] D.D. Burduhos, M.M.A.B. Abdullah, P. Vizureanu, The effect of fly ash/alkaline activator ratio in Class F fly ash based geopolymers, Eur. J. Mater. Sci. Eng. **2**, 111-118 (2017).

[6] H. Ng, C.Y. Heah, M.M.A.B. Abdullah, Y. Ng, R. Bayuaji, Study of fly ash geopolymer and fly ash/slag geopolymer in term of physical and mechanical properties, Eur. J. Mater. Sci. Eng. **5**, 187-198 (2020).

[7] E.A. Obonyo, E. Kamseu, P.N. Lemougna, A.B. Tchamba, U.C. Melo, C. Leonelli, A sustainable approach for the geopolymerization of natural iron-rich aluminosilicate materials, Sustainability (Switzerland) **6**, 5535-5553 (2014).

[8] C.Y. Heah, H. Kamarudin, A.M. Mustafa Al Bakri, Kaolin-based geopolymers with various NaOH concentrations, Int. J. Miner. Metall. Mater. **20**, 313-322 (2013).

[9] F.U.A. Shaikh, Mechanical and durability properties of fly ash geopolymer concrete containing recycled coarse aggregates, Int. J. Sustain. Built Environ. **5**, 277-287 (2016).

[10] A.A. Paizun, M. Fathullah, M.M.A. Abdullah, Z. Shayfull, F. Tahir, A short review on fly ash geopolymer machining: A large gap with bright potential for engineering applications, International Conference on Green Design and Manufacture (IConGDM2019), AIP Conference Proceedings, pp. 020184 (2019).

[11] G.S. Ryu, Y.B. Lee, K.T. Koh, Y.S. Chung, The mechanical properties of fly ash-based geopolymer concrete with alkaline activators, Constr. Build. Mater. **47**, 409-418 (2013).

[12] W. Bin Sun, Y. Jiang, W.Z. He, An overview on the blast loading and blast effects on the RC structures, Appl. Mech. Mater. **94**, 77-80 (2011).

[13] C.F. Zhao, J.Y. Chen, Y. Wang, S.J. Lu, Damage mechanism and response of reinforced concrete containment structure under internal blast loading, Theor. Appl. Fract. Mech. **61**, 12-20 (2012).

[14] Q. Ling, Y. He, Y. He, C. Pang, Dynamic response of multibody structure subjected to blast loading, Eur. J. Mech. A/Solids **64**, 46-57 (2017).

[15] R. Jayasooriya, D.P. Thambiratnam, N.J. Perera, V. Kosse, Blast response and safety evaluation of a composite column for use as key element in structural systems, Eng. Struct. **33**, 3483-3495 (2011).

[16] C. Wu, M. Lukaszewicz, K. Schebella, L. Antanovskii, Experimental and numerical investigation of confined explosion in a blast chamber, J. Loss Prev. Process Ind. **26**, 737-750 (2013).

[17] R. Castedo, P. Segarra, A. Alanon, L.M. Lopez, A.P. Santos, J.A. Sanchidrian, Air blast resistance of full-scale slabs with different compositions: Numerical modeling and field validation, Int. J. Impact Eng. **86**, 145-156 (2015).

[18] C. Diyaroglu, E. Oterkus, E. Madenci, T. Rabczuk, A. Siddiq, Peridynamic modeling of composite laminates under explosive loading, Compos. Struct. **144**, 14-23 (2016).

[19] K. Mahmadi, N. Aquelet, Euler-Lagrange simulation of high pressure shock waves, Wave Motion **54**, 28-42 (2015).

[20] D. Angela, D.D. Angela, Finite element analysis of fatigue response of nickel steel compact tension samples using ABAQUS, Procedia Structural Integrity **13**, 939-946 (2018).

[21] N.F. Hany, E.G. Hantouche, M.H. Harajli, Finite element modeling of FRP-confined concrete using modified concrete damaged plasticity, Eng. Struct. **125**, 1-14 (2016).

[22] Abaqus Analysis User Manual – Abaqus Version 6.8. (2008). Retrieved November 5, 2010, from http://bee-pg-031941:2080/v6.8/books/usb/default.htm